J|A|C|S
ARTICLES
Published on Web 11/19/2003

# Electronic Structure of 1 to 2 nm Diameter Silicon Core/Shell Nanocrystals: Surface Chemistry, Optical Spectra, Charge Transfer, and Doping

Zhiyong Zhou, Richard A. Friesner, and Louis Brus*

*Contribution from the Chemistry Department, Columbia University, New York, New York 10027*

Received May 30, 2003; E-mail: brus@chem.columbia.edu

***Abstract:*** Static and time-dependent density functional calculations, geometrically optimized and including all electrons, are described for silicon nanocrystals as large as $Si_{87}H_{76}$, which contains 163 atoms. We explore and predict the effect that different $sp^3$ passivation schemes—F or H termination, thin oxide shell, or alkane termination—have on the HOMO and LUMO, on the optical spectra, and on electron transfer properties. Electronegativity comparisons are a useful guide in understanding the observed deviation from the simple quantum size effect model. Nanocrystals containing Al or P impurity atoms, either on the surface or in the interior, are explored to understand electrical doping in strongly quantum-confined nanocrystals. Surface dangling bonds are found to participate in internal charge transfer with P atom dopant electrons.

## Introduction

Silicon transistors are moving toward dimensions of just a few nanometers, and there are new device designs (for example, single-electron transistors and floating-gate memory[1]) which incorporate Si nanocrystals. There has also been extensive experimental work on understanding the high luminescence quantum yield of Si nanocrystals as compared with bulk crystalline Si.[2] Optical gain was recently reported for Si nanocrystals in a silica thin film,[3] which suggests that Si nanocrystal materials may yet introduce optical functionality into silicon microelectronics processing. Yet, it remains very difficult to synthesize or characterize monodisperse homogeneous small Si nanocrystals. Many workers try to characterize single silicon nanocrystals rather than the ensemble, because the structural, stoichiometric, and photophysical property distributions are large in real samples.[4,5] In studies of nanocrystal inclusions in silica thin films, characterization of the buried particles is especially difficult. Thus, our knowledge of small Si nanocrystals is poor. In this paper, we attempt to understand and predict electrical properties using ab initio electronic structure theory. We now describe surface passivation, P and Al doping, optical excitation, and charge-transfer properties of nanocrystals based upon $Si_{35}$, $Si_{66}$, and $Si_{87}$ cores. Our comparison of H atom and oxide shell passivation has been given earlier.[6]

As nanocrystals grow in size, they evolve from being molecular-like to being solid state-like. At larger sizes, the quantum size effect model combined with simple continuum electrostatics,[7,8] the empirical tight-binding model,[9,10] and empirical pseudopotentials (including schematic passivation changes) at fixed geometry,[11−15] all give good insight. As might be expected, in the 1−2 nm size regime, the molecular aspects are dominant, and these models often fail. For H passivated Si clusters in this size regime, ab initio pseudopotentials with time-dependent LDA have been used to predict optical spectra.[16,17] The effect of several O atom surface "defects" has also been carefully explored.[18]

We employ ab initio Density Functional Theory (DFT) methodologies that have been developed for large, low-symmetry molecules such as proteins. In the past decade, ab initio calculations have significantly advanced due to the following: (a) the increase in speed and decrease in cost of PC computers, (b) a major increase in algorithm coding efficiency, and (c) progress in the fundamental understanding of the exchange-correlation functional. These advances make it possible to do ab initio all-electron calculations (of calibrated and understood accuracy) with complete geometrical optimization on species with several hundred atoms.

(1) Ostraat, M. L.; De Blauwe, J. W.; Green, M. L.; Bell, L. D.; Brongersma, M. L.; Casperson, J.; Flagan, R. C.; Atwater, H. A. *Appl. Phys. Lett.* **2001**, *79*, 433.
(2) Several reviews of nanocrystal optical properties appear in: *Light Emission in Silicon*, *Volume 49 of Semiconductors and Semimetals*; Lockwood, D., Ed.; Academic Press: New York, 1998.
(3) Dal Negro, L.; Cazzanelli, M.; Daldosso, N.; Gaburro, Z.; Pavesi, L.; Priolo, F.; Pacifici, D.; Franzo, G.; Iacona, F. *Physica E* **2003**, *16*, 297.
(4) Credo, G. M.; Mason, M. D.; Buratto, S. K. *Appl. Phys. Lett.* **1999**, *74*, 1978.
(5) Valenta, J.; Juhasz, R.; Linnros, J. *Appl. Phys. Lett.* **2002**, *80*, 1070.
(6) Zhou, Z. Y.; Brus, L.; Friesner, R. *Nano Lett.* **2003**, *3*, 163.
(7) Brus, L. E. *J. Chem. Phys.* **1983**, *79*, 5566.
(8) Allan, G.; Delerue, C.; Lannoo, M.; Martin, E. *Phys. Rev. B* **1995**, *52*, 11 982.
(9) Proot, J. P.; Delerue, C.; Allan, G. *Appl. Phys. Lett.* **1992**, *61*, 1948.
(10) Leung, K.; Whaley, K. B. *Phys. Rev. B* **1997**, *56*, 7455.
(11) Krishna, M. V. R.; Friesner, R. A. *Phys. Rev. Lett.* **1991**, *67*, 629.
(12) Krishna, M. V. R.; Friesner, R. A. *J. Chem. Phys.* **1991**, *95*, 8309.
(13) Krishna, M. V. R.; Friesner, R. A. *J. Chem. Phys.* **1992**, *96*, 873.
(14) Reboredo, F. A.; Franceschetti, A.; Zunger, A. *Phys. Rev. B* **2000**, *61*, 13 073.
(15) Reboredo, F. A.; Zunger, A. *Phys. Rev. B* **2001**, *63*, 235314.
(16) Vasiliev, I.; Ogut, S.; Chelikowsky, J. R. *Phys. Rev. Lett.* **2001**, *86*, 1813.
(17) Vasiliev, I.; Ogut, S.; Chelikowsky, J. R. *Phys. Rev. B* **2002**, *65*, 115 416.
(18) Vasiliev, I.; Chelikowsky, J. R.; Martin, R. M. *Phys. Rev. B* **2002**, *65*, 121302.

***Table 1.*** Calculated Optical Transitions of $Si_{35}H_{36}$ and $Si_{35}(OH)_{36}$ with Different Methods[a]

| $Si_{35}H_{36}$ | | | | | $Si_{35}(OH)_{36}$ | | | | |
|---|---|---|---|---|---|---|---|---|---|
| static DFT | | TDDFT | | | static DFT | | TDDFT | | |
| singlet | | singlet | | triplet | singlet | | singlet | | triplet |
| energy (eV) | oscillator strength | energy (eV) | oscillator strength | energy (eV) | energy (eV) | oscillator strength | energy (eV) | oscillator strength | energy (eV) |
| 5.00 | 0.0069 | 4.47 | 0.0011 | 4.29 | 2.73 | 0.0000 | 2.13 | 0.0000 | 2.07 |
| 5.07 | 0.0000 | 4.52 | 0.0000 | 4.35 | 2.87 | 0.0000 | 2.23 | 0.0000 | 2.17 |
| 5.11 | 0.1310 | 4.54 | 0.0000 | 4.39 | 2.99 | 0.0000 | 2.33 | 0.0000 | 2.26 |
| 5.14 | 0.0005 | 4.54 | 0.0022 | 4.40 | 3.74 | 0.0024 | 2.91 | 0.0001 | 2.80 |
| 5.18 | 0.0306 | 4.56 | 0.0090 | 4.42 | 3.88 | 0.0000 | | | |
| 5.21 | 0.2153 | | | 4.44 | 4.00 | 0.0172 | | | |

[a] B3LYP functional is used in both DFT methods. Both calculations are based on the same geometry optimized from static DFT at 6-31G* level. The final energies and oscillator strengths of static DFT are calculated at the cc-pVTZ(-f) level and those of TDDFT are calculated at 6-31G* level.

**Comparison between DFT and TDDFT Calculations.** Hybrid DFT functionals, such as B3LYP, which combine nonlocal exact Hartree−Fock exchange with the generalized gradient approximation have "changed the entire landscape of quantum chemistry".[19] Becke invented this class of functional to reproduce absolute bond energies and ionization potentials in a small molecule test set to within chemical accuracy (ca. 3 kcal/mol or 0.13 eV).[20] More recently in bulk crystals, it was found that hybrid functionals in static DFT quantitatively reproduce the band structure and indirect gap of crystalline Si, and the band gaps of complex crystalline oxides such as $La_2CuO_4$, $Cr_2O_3$, NiO, $TiO_2$, and $UO_2$.[21−23] In these oxides especially, earlier functionals often gave qualitatively incorrect (metallic) results.

All-electron static B3LYP DFT calculations were performed using the Jaguar 4.0 and 5.0 codes[24] from Schrodinger Inc. with an atom-centered basis set and complete geometrical optimization. As an example, the calculation of the internal P-doped, H-passivated $Si_{66}$ species took 76 h on a 1.4 GHz Pentium III single processor IBM PC with a 6-31 g* basis set in Jaguar 5.0, when started from the geometry of $Si_{66}H_{64}$. In the case of the ions, we reoptimized the structures in the presence (or absence) of the extra charge. The vertical ionization potential refers to the total energy difference when the ion is converged for the fixed geometry of the neutral. The adiabatic ionization potential is the energy difference when the ion is also geometrically optimized. The difference of the two ionization energies is the hole reorganization energy, which is important in Marcus−Hush electron-transfer rate theory.

As described above, static B3LYP in crystals can give single electron promotion energies that are close to the experimental band gap optical transitions. The HOMO−LUMO gap in static DFT does not include interaction between excited configurations, and electron−hole exchange. Within linear response theory these effects are included in time dependent DFT (TDDFT) for vertical excitation at the ground state geometry. The experimental optical spectra of many large planar aromatic molecules have been accurately reproduced with TDDFT.[25−29] In addition, localized defect optical transitions in silica[30] are accurately modeled with TDDFT. Here, a careful study showed that nonhybrid functionals give a significantly worse results.

In nanocrystals, optical spectra are less well-known, and thus, the accuracy of theoretical methods is more difficult to assess. In the case of the H-passivated $Si_{35}H_{36}$ nanocrystal, Garoufalis, Zdetsis, and Grimme (GZG) report that the TD DFT lowest singlet is ca. 13% lower than the static HOMO−LUMO gap.[31] Using the Tamm−Dancoff TDDFT code in Q-chem version 2.0[32] with a 6-31 g* basis, we have calculated low-lying singlet and triplet states in Table 1. These TDDFT results confirm the important static DFT result that the lowest singlet transitions are mostly dipole allowed in $Si_{35}H_{36}$ and dipole forbidden in $Si_{35}(OH)_{36}$. In agreement with GZG, the lowest singlet transition in lies about 0.5 eV below the static HOMO−LUMO gap; in the oxide species, we find the difference is about 0.6 eV. At present, the differences between DFT and TDDFT transition energies represents uncertainty in prediction of nanocrystal optical spectra. In this connection, Williamson et al.[33] show for H termination that static B3LYP transition energies are actually closer to many body, time-consuming excited-state quantum Monte Carlo energies than are the TDDFT energies.

**Surface Passivation: Optical Spectra and Fermi Energies.** We explore four different chemical passivation schemes involving interface continuation of the Si $sp^3$ hybridization: H and F atom bonding to Si, a thin $SiO_2$ oxide shell as made by brief high-temperature oxidation, and Si−C hydrocarbon ligands. The hydrocarbon termination also serves as a model for thin SiC shell passivation. In each case, we are considering core/shell, (i.e., not single defect) structures, and in each case, we find the HOMO and LUMO to be strongly delocalized. The effect of nonpolar H atom bonding is understood in broad outline in prior work. Thin oxide shell passivation is chemically more stable

(19) Raghavachari, K. *Theor. Chem. Acc.* **2000**, *103*, 361.
(20) Becke, A. D. *J. Chem. Phys.* **1993**, *98*, 5648.
(21) Muscat, J.; Wander, A.; Harrison, N. M. *Chem. Phys. Lett.* **2001**, *342*, 397.
(22) Perry, J. K.; Tahir-Kheli, J.; Goddard, W. A. *Phys. Rev. B* **2002**, *65*, 144 501.
(23) Kudin, K. N.; Scuseria, G. E.; Martin, R. L. *Phys. Rev. Lett.* **2002**, *89*, 266402.
(24) Jaguar 4.0 and 5.0, Schrodinger, L. L. C., Portland, OR, 1991−2003.
(25) Stratmann, R. E.; Scuseria, G. E.; Frisch, M. J. *J. Chem. Phys.* **1998**, *109*, 8218.
(26) Hirata, S.; Lee, T. J.; Head-Gordon, M. *J. Chem. Phys.* **1999**, *111*, 8904.
(27) Pogantsch, A.; Heimel, G.; Zojer, E. *J. Chem. Phys.* **2002**, *117*, 5921.
(28) Neiss, C.; Saalfrank, P.; Parac, M.; Grimme, S. *J. Phys. Chem. A* **2003**, *107*, 140.
(29) Halasinski, T. M.; Weisman, J. L.; Ruiterkamp, R.; Lee, T. J.; Salama, F.; Head-Gordon, M. *J. Phys. Chem. A* **2003**, *107*, 3660.
(30) Raghavachari, K.; Ricci, D.; Pacchioni, G. *J. Chem. Phys.* **2002**, *116*, 825.
(31) Garoufalis, C. S.; Zdetsis, D.; Grimme, S. *Phys. Rev. Lett.* **2001**, *87*, 276 402.
(32) Kong, J.; White, C. A.; Krylov, A. I.; Sherrill, D.; Adamson, R. D.; Furlani, T. R.; Lee, M. S.; Lee, A. M.; Gwaltney, S. R.; Adams, T. R.; Ochsenfeld, C.; Gilbert, A. T. B.; Kedziora, G. S.; Rassolov, V. A.; Maurice, D. R.; Nair, N.; Shao, Y.; Besley, N. A.; Maslen, P. E.; Dombroski, J. P.; Daschel, H.; Zhang, W.; Korambath, P. P.; Baker, J.; Byrd, E. F. C.; Van Voorhis, T.; Oumi, M.; Hirata, S.; Hsu, C.-P.; Ishikawa, N.; Florian, J.; Warshel, A.; Johnson, B. G.; Gill, P. M. W.; Head-Gordon, M.; Pople, J. A. Q-Chem 2.0: A high-performance ab initio electronic structure program, *J. Comput. Chem.* **2000**, *21*, 1532−1548.
(33) Williamson, A. J.; Grossman, J. C.; Hood, R. Q.; Puzder, A.; Galli, G. *Phys. Rev. Lett.* **2002**, *89*, 196803.

***Table 2.*** Properties of Structurally Optimized Species as Described in the Text[a]

| species | $Si_{10}H_{16}$ | $Si_{10}(OH)_{16}$ | $Si_{10}F_{16}$ | $Si_{35}H_{36}$ | $Si_{35}(OH)_{36}$ | $Si_{35}F_{36}$ | $Si_{29}O_6(OH)_{24}$ |
|---|---|---|---|---|---|---|---|
| symmetry of optimized species | Td | Td | Td | Td | Td | Td | D2 |
| HOMO | −7.58 | −4.79 | −8.20 | −6.81 | −5.75 | −8.14 | −5.65 |
| symmetry of HOMO | T1 | T1 | T1 | T2 | T1 | T1 | B1 |
| LUMO | −1.13 | −1.69 | −4.76 | −1.81 | −3.03 | −4.94 | −2.77 |
| symmetry of LUMO | A1 | A1 | A1 | A1 | A1 | A1 | A |
| LUMO−HOMO gap | 6.45 | 3.09 | 3.44 | 5.00 | 2.73 | 3.20 | 2.88 |
| adiabatic ionization energy $\mathbf{I_a}$ | 8.81 | 5.88 | 9.45 | 7.60 | 6.40 | 8.96 | 6.40 |
| vertical ionization energy $\mathbf{I_v}$ | 8.98 | 6.14 | 9.70 | 7.73 | 6.68 | 9.14 | 6.64 |
| hole reorganization energy $\lambda_h$ | 0.17 | 0.26 | 0.24 | 0.13 | 0.28 | 0.18 | 0.24 |
| adiabatic electron affinity $\mathbf{A_a}$ | −0.01 | 0.64 | 3.45 | 0.98 | 2.16 | 4.03 | 1.91 |
| vertical electron affinity $\mathbf{A_v}$ | −0.17 | 0.45 | 3.33 | 0.89 | 2.15 | 3.98 | 1.82 |
| electron reorganization energy $\lambda_e$ | 0.16 | 0.19 | 0.12 | 0.08 | 0.01 | 0.05 | 0.09 |
| Fermi energy | −4.40 | −3.29 | −6.51 | −4.31 | −4.42 | −6.56 | −4.23 |
| absolute hardness | 9.15 | 5.69 | 6.37 | 6.84 | 4.53 | 5.15 | 4.82 |
| dipole moment (Debye) | 0.00 | 0.00 | 0.00 | 0.00 | 0.00 | 0.00 | 0.00 |
| quadrupole moment(xx) (Debye·Å) | −16.1 | 22.9 | −44.8 | −58.4 | −21.8 | −154.9 | −23.5 |

| species | $Si_{29}(CH_2)_6(CH_3)_{24}$ | $Si_{35}O_{24}(SiH_2)_{12}(OH)_{12}$ | $Si_{66}H_{64}$ | $Si_{66}F_{64}$ | $Si_{66}O_{12}(OH)_{40}$ | $Si_{87}H_{76}$ |
|---|---|---|---|---|---|---|
| symmetry of optimized species | Td | C3 | Td | Td | C1 | Td |
| HOMO | −5.61 | −6.19 | −6.53 | −7.72 | −5.56 | −6.12 |
| symmetry of HOMO | T1 | A | T2 | T1 | A1 | T2 |
| LUMO | −1.21 | −3.06 | −2.29 | −4.21 | −2.54 | −2.08 |
| symmetry of LUMO | A1 | A | A1 | A1 | A1 | E |
| LUMO−HOMO gap | 4.40 | 3.13 | 4.24 | 3.52 | 3.02 | 4.04 |
| adiabatic ionization energy $\mathbf{I_a}$ | 6.42 | 6.68 | 7.50 | 8.46 | / | 6.81 |
| vertical ionization energy $\mathbf{I_v}$ | 6.46 | 7.07 | 7.56 | 8.87 | 6.36 | 6.88 |
| hole reorganization energy $\lambda_h$ | 0.04 | 0.39 | 0.06 | 0.41 | / | 0.08 |
| adiabatic electron affinity $\mathbf{A_a}$ | 0.37 | 2.30 | 1.46 | 3.13 | / | 1.38 |
| vertical electron affinity $\mathbf{A_v}$ | 0.36 | 2.23 | 1.42 | 3.07 | 1.74 | 1.30 |
| electron reorganization energy $\lambda_e$ | 0.01 | 0.06 | 0.04 | 0.06 | / | 0.08 |
| Fermi energy | −3.41 | −4.65 | −4.48 | −5.97 | −4.05 | −4.09 |
| absolute hardness | 6.10 | 4.84 | 6.04 | 5.81 | 4.62 | 5.58 |
| dipole moment (Debye) | 0.00 | 4.66 | 0.00 | 0.00 | 6.56 | 0.00 |
| quadrupole moment(xx) (Debye·Å) | −5.4 | −96.7 | −76.84 | −262.3 | −76.6 | −98.1 |

[a] All energies are in eV. $Si_{66}O_{12}(OH)_{40}$ was optimized at 3-21G level, with final energies calculated at the 6-31G* level. $Si_{66}F_{64}$ and $Si_{87}H_{76}$ was optimized at 6-31G* level, with final energies also calculated at the 6-31G* level. Other species were optimized at the 6-31G* level, with final energies calculated at the cc-pVTZ(-f) level.

than H passivation and is likely to be important in practical devices. Oxide and SiC shells introduce questions of strain at the interface.

Table 2 shows calculated properties as a function of passivation and size. Our results for H passivation are consistent with those of Williamson et al.[33] with B3LYP. If we compare H versus F termination, then we see that a major effect of the polar Si−F surface bonding is to increase the surface dipole and thus to lower the Fermi energy $-(I + A)/2$ with respect to H termination. For the $Si_{35}$ species, the Fermi level decreases from −4.31 eV to −6.56 eV. The adiabatic electron affinity increases by a factor of 4, from 0.98 to 4.03 eV. Both HOMO and LUMO shift negative because of the electronegativity of F, but the shift is not equal. The LUMO shifts negatively more than the HOMO, and thus the band gap decreases from 5.00 eV in $Si_{35}H_{36}$ to 3.20 eV in $Si_{35}F_{36}$. The calculated static optical transitions for F termination appear in the Supporting Information.

The relative influence of passivation with F is higher in the smaller nanocrystal sizes as would be expected from simple stoichometry. This causes the band gap for F-termination to deviate strongly from the simple quantum size effect observed with H-passivation, and to be relatively flat with size, as shown in Figure 1. For the $Si_{66}$, $Si_{35}$, and $Si_{10}$ species, the band gaps are 3.52, 3.20, and 3.44 eV, respectively. For H-termination, the corresponding gaps are 4.24, 5.00, and 6.45 eV, respectively. The vertical $I$ and $A$ values for F-termination show a similar flat dependence.

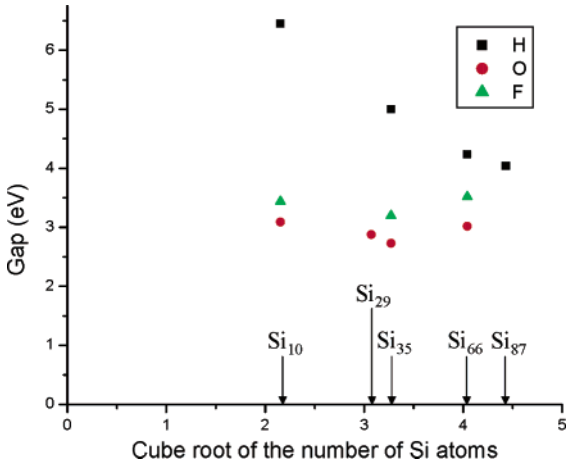


***Figure 1.*** HOMO−LUMO gap of Si nanocrystals with different size and passivation.

The influence of electronegative F is apparent in the HOMO and LUMO shown in Figure 2 for the $Si_{66}$ species. The H HOMO shows regions of high density inside the nanocrystal as expected for 1S type quantum size effect wave functions. In the F species, the HOMO symmetry changes from T2 to T1, and the density resides mostly on surface Si−Si bonds connected to Si atoms that are also bonded to F. These surface Si−Si bonds are weakened "back-bonds" created by the strong polar bonds to F.

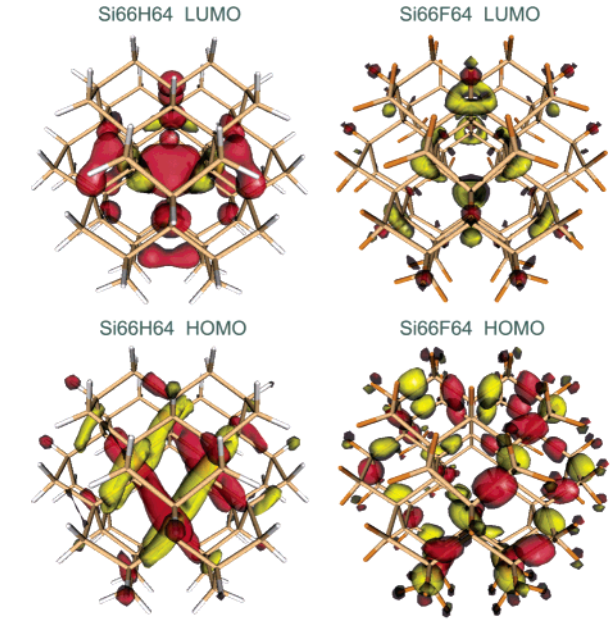


***Figure 2.*** HOMO and LUMO of $Si_{66}H_{64}$ and $Si_{66}F_{64}$.

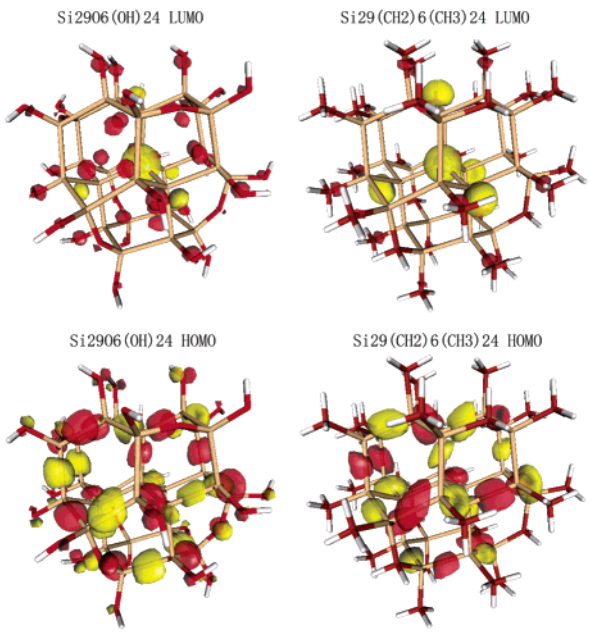


***Figure 3.*** HOMO and LUMO of $Si_{29}O_6(OH)_{24}$ and $Si_{29}(CH_2)_6(CH_3)_{24}$.

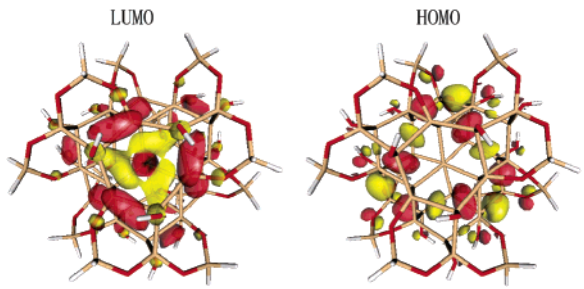


***Figure 4.*** HOMO and LUMO of $Si_{35}O_{24}(SiH_2)_{12}(OH)_{12}$.

Although polar F passivation increases the surface dipole and lowers the Fermi energy, hydrocarbon passivation lowers the dipole and increases the Fermi energy. For $Si_{29}(CH_2)_6(CH_3)_{24}$, the Fermi energy increases to −3.41 eV compared with −4.31 eV in $Si_{35}H_{36}$. The vertical electron affinity is only slightly positive at 0.36 eV, and there is a small 0.6 eV decrease in the band gap as compared with H termination. The predicted 4.4-eV static gap is consistent with a report that Si particles with Si−C alkane surface bonds strongly luminescence in the blue.[34] Structurally, this species is somewhat similar to previously described $Si_{29}O_6(OH)_{24}$.[6] On the small, flat 111 facets of this initially octahedral nanocrystal, each surface Si is terminated with a $CH_3$ group. At the six vertexes where facets meet, two Si atoms are bridged by one methylene $CH_2$ group. The Si−Si distance shortens by 0.423 Å when bridged by methylene. As in the oxide, the HOMO and LUMO remain delocalized despite this strain. Figure 3 compares the HOMO and LUMO of these two species. The distribution over different atom types is very similar to each other. In the HOMO, about 3% of the density resides on the bridging $CH_2$ group. The lowest singlet transition at 4.40 eV is forbidden, but there is a strong optical transition lying 0.24 eV above it. Calculated static optical transitions appear in the Supporting Information.

As described in detail in our earlier paper,[6] oxide passivation creates a specific chemical interaction which pushes the HOMO up and the LUMO down, while leaving the Fermi energy essentially unchanged (Table 2). As in F case, the HOMO is drawn toward those Si atoms at vertexes that are bonded to two electronegative (F or O) atoms. This substantial band gap change between oxide and H passivation explains the experimental observation that 1−2 nm H terminated Si particles emit in the ultraviolet-blue region, whereas oxide terminated particles emit in the yellow-red. In an important experiment, Mizuno, Koyama, and Koshida showed that blue photoemission from porous silicon is due to small H-terminated nanocrystals without any detectible oxide.[35] If these particles are exposed to air, they oxidize in a few minutes, and emit in the yellow-red,[36] similar to the emission of aerosol Si nanocrystals with a thin oxide shell made at high temperature.[37] Kanemitsu has also carefully demonstrated that the band gaps of oxide core/shell particles are much smaller than those for H-termination.[38]

We represent an oxide shell of several $SiO_2$ layers by simple OH surface termination. On 111 facets in the $Si_{35}$ species, we have explored the effect of oxide thickness by replacing two neighboring hydroxyl H atoms with a $SiH_2$ bridging group between the O atoms as shown in Figure 4. In this species, $Si_{35}O_{24}(SiH_2)_{12}(OH)_{12}$, we observe its band gap increases to 3.13 eV from 2.73 eV in $Si_{35}(OH)_{36}$. Only 1% of HOMO density and 5% of LUMO density are on 12 newly added outer Si atoms. Most of the HOMO density resides on the interfacial Si−Si bonds, which is similar to $Si_{35}(OH)_{36}$. The optical transitions near the band gap are weakly allowed with microsecond time scale lifetime (Supporting Information). The approximation of representing an oxide shell of several $SiO_2$ layers by simple OH surface termination is a reasonable first step.

The previously reported static transition energies and oscillator strengths for $Si_{35}$ and $Si_{66}$ species (Supporting Information,

(34) Holmes, J. D.; Ziegler, K. J.; Doty, R. C.; Pell, L. E.; Johnston, K. P.; Korgel, B. A. *J. Am. Chem. Soc.* **2001**, *123*, 3743.
(35) Mizuno, H.; Koyama, H.; Koshida, N. *Appl. Phys. Lett.* **1996**, *69*, 3779.
(36) Wolkin, M. V.; Jorne, J.; Fauchet, P. M.; Allan, G.; Delerue, C. *Phys. Rev. Lett.* **1999**, *82*, 197.
(37) Wilson, W. L.; Szajowski, P. F.; Brus, L. E. *Science* **1993**, *262*, 1242.
(38) Kanemitsu, Y.; Okamoto, S. *Phys. Rev. B* **1998**, *58*, 9652.

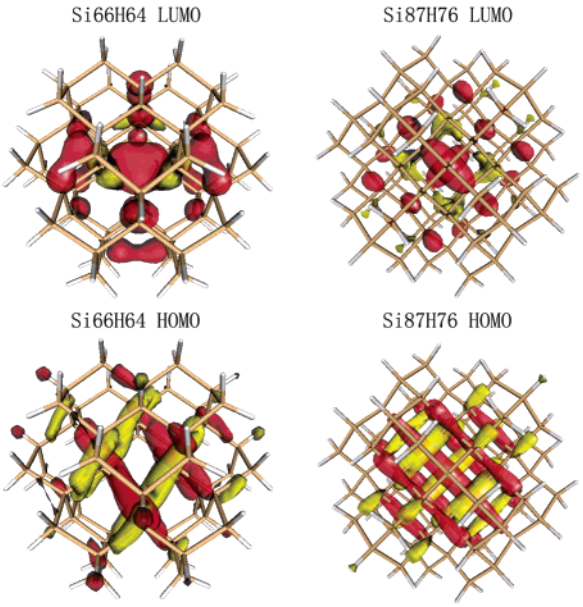


***Figure 5.*** HOMO and LUMO of $Si_{66}H_{64}$ and $Si_{87}H_{76}$.

earlier publication[6]) indicate that the lowest singlet for H termination is likely dipole allowed, and for oxide termination likely dipole forbidden. As mention above, this is supported by TDDFT results for $Si_{35}$ species. Figure 5 compares the HOMO and LUMO spatial distribution of the $Si_{66}$ and $Si_{87}$ H terminated species. In the $Si_{66}$ HOMO 32% of the density resides on interior Si atoms, and in $Si_{87}$ 64%. The density moves inward as size increases; in the simple quantum size effect model both HOMO and LUMO have nodes on the surface. Also, the transition should be systematically dipole forbidden in larger species as bulk Si is approached. We find in both species there are several nearly degenerate LUMO orbitals. As shown in the Supporting Information, three band gap optical transitions are predicted within 0.05 eV of 4.08 eV; two of the three are dipole allowed with microsecond time scale lifetimes. Two significantly stronger transitions lie 0.2 eV higher. $Si_{87}H_{76}$ still has significantly allowed character.

The excited state (exciton) singlet−triplet exchange splitting in bulk Si is only 0.15meV, due to the large physical size of the exciton. In optically excited 3−4 nm diameter H terminated nanocrystals in porous silicon, which emit near 1.8 eV, the splitting increases to several meV, as shown in magnetooptic experiments.[39,40] In this size range, the exchange splitting is on the order of *kT* (about 25 meV) at 23 °C, and there is a dynamic population equilibrium between these two components of the excited state. The splitting increases rapidly in smaller nanocrystals with larger confinement effects. With TDDFT in Table 1 we calculate that the splitting between the lowest singlet and lowest triplet in $Si_{35}H_{36}$ is 180 meV, and in the oxide 60 meV. In 1−2 nm Si nanocrystals, crossing into the triplet would be almost irreversible at room temperature because of the large splitting. The intersystem crossing yield into the lowest triplet remains unknown. Using a molecular analogy, the crossing rate should decrease as the singlet−triplet energy gap increases. In the H terminated species, the strong blue emission that is experimentally observed suggests that the singlet state is emitting.

**Charge-Transfer Involving Nanocrystals.** Geometrically optimized calculations on nanocrystal cations and anions provide essential parameters for modeling the rates of electron-transfer reactions. The difference between the vertical and adiabatic electron affinity in Table 2 is the reorganization energy $\lambda_e$ of an extra electron—the (positive) Franck−Condon energy released when the nanocrystal relaxes from the neutral to the equilibrium anion structure. In bulk silicon and larger nanocrystals, these energies are small, on the order of a few meV, because of the weak vibronic coupling present in nonpolar crystalline Si.[41] The Marcus−Hush weak-coupling electron-transfer rate varies as[42,43]

$$k_{et} = \frac{2\pi H_{DA}^{\,2}}{h}\left[\frac{\pi}{\lambda k_B T}\right]^{1/2} \exp\left[-\frac{(\lambda + \Delta G)^2}{4\lambda k_B T}\right]$$

Here, $\lambda$ is the sum of the donor and acceptor reorganization energies, and $\Delta G$ is the exothermicity. For fast barrierless transfer, $-\Delta G$ must equal $\lambda$. When $\lambda = 0$, resonant electronic tunneling occurs without motion of nuclei. Table 2 shows that $\lambda_e$ in $Si_{29}$ and larger species with polar surfaces tends to be a few tens of meV for electrons, and perhaps 2−3 times larger for holes. In the H and alkane terminated nanocrystals, the numbers tend to be smaller. These magnitudes will modestly affect the rates of transfer as compared with purely resonant tunneling. Although there is an effect which tends to increase in the presence of polar bonds, the effect is not strong in these cases of delocalized wave functions. There is not much reorganization—the singly occupied HOMO of the anion is very similar to the LUMO of the neutral. However, the small values of the Si nanocrystal $\lambda$ imply that the transfer rate is quite sensitive to the polarity of the surrounding dielectric—an effect which has been observed in porous silicon films.[41]

**Incomplete Passivation, Luminescence Quenching, and Charge Trapping. A. Surface Dangling Bond.** In experimental samples, some particles show high (approaching 100%) luminescence quantum yields and other particles show essentially zero quantum yields. High luminescence particles are assumed to be completely passivated. Other particles have one (or more) surface dangling bonds (a "defect" or radical) which has been calculated to quench band gap luminescence.[44] Ensemble ESR measurements do show dangling bond signals.[45] Forming gas reaction with silica films containing such nanocrystals decreases the ESR intensity, and markedly increases luminescence intensity, in agreement with this hypothesis.[46,47] (In microelectronics, forming gas reaction passivates dangling bonds at the silicon: silica interface with H atoms). In porous silicon samples

(39) Diener, J.; Kovalev, D.; Heckler, H.; Polisski, C.; Koch, F. *Phys. Rev. B* **2001**, *63*, 073 302.
(40) Kovalev, D.; Heckler, H.; Polisski, G.; Diener, J.; Koch, F. *Opt. Mater.* **2001**, *17*, 35.
(41) Brus, L. *Phys. Rev. B* **1996**, *53*, 4649.
(42) Marcus, R. A.; Sutin, N. *Biochim. Biophys. Acta* **1985**, *811*, 265.
(43) For a review of electron transfer issues, see: Adams, D. M.; Brus, L.; Chidsey, C. E. D.; Creager, S.; Creutz, C.; Kagan, C. R.; Kamat, P. V.; Lieberman, M.; Lindsay, S.; Marcus, R. A.; Metzger, R. M.; Michel-Beyerle, M. E.; Miller, J. R.; Newton, M. D.; Rolison, D. R.; Sankey, O.; Schanze, K. S.; Yardley, J.; Zhu, X. Y. Charge transfer on the nanoscale: Current status. *J. Phys. Chem. B* **2003**, *107*, 6668.
(44) Delerue, C.; Allan, G.; Lannoo, M. *Phys. Rev. B* **1993**, *48*, 11 024.
(45) Brandt, M. S.; Stutzmann, M. *Appl. Phys. Lett.* **1992**, *61*, 2569.
(46) Lopez, M.; Garrido, B.; Garcia, C.; Pellegrino, P.; Perez-Rodriguez, A.; Morante, J. R.; Bonafos, C.; Carrada, M.; Claverie, A. *Appl. Phys. Lett.* **2002**, *80*, 1637.
(47) Pellegrino, P.; Garrido, B.; Garcia, C.; Ferre, R.; Moreno, J. A.; Morante, J. R. *Physica E* **2003**, *16*, 424.

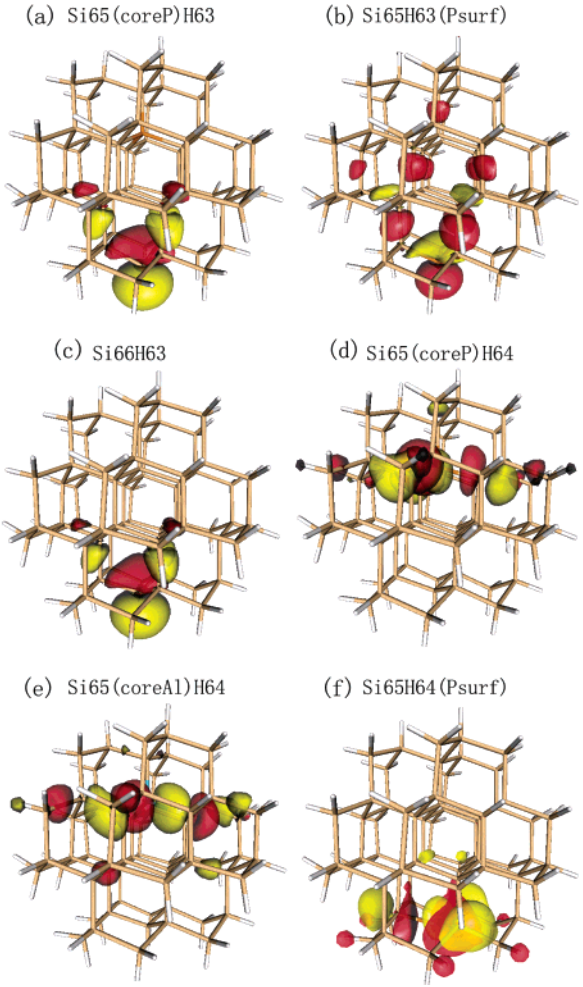


***Figure 6.*** HOMO of doped $Si_{66}$ nanocrystals.

containing a wide size range of H passivated nanocrystals, the dangling bond ESR signal is also observed. Here, optical-magnetic double resonance experiments show a direct kinetic connection between luminescence quenching and the dangling bond.[48] Nanocrystals with dangling bonds show an 0.9 eV infrared emission at low temperature; this transition is not characteristic of a well passivated nanocrystal.[49]

In $Si_{66}H_{63}$, we remove one H atom at the center of a 111 facet, creating a "radical nanocrystal" with an odd number of electrons. As expected from chemical intuition, the missing H atom creates a singly occupied p-like "defect" state (Figure 6c) localized on the uncapped Si, lying in the gap 0.85 eV above the T2 HOMO of the parent $Si_{66}H_{64}$ nanocrystal as shown in Figure 7. If we add an extra electron to this radical, i.e., form the $Si_{66}H_{63}$ radical anion the HOMO is a singlet lone pair on the uncapped surface Si, lying 1.41 eV above the delocalized orbital corresponding to the parent nanocrystal HOMO. If an electron is removed to form the radical cation, the empty lone pair oribital is nearly mid-gap, about 2.2 eV above the delocalized HOMO. The relative energies of these orbitals are shown in Figure 7.

Figure 8 shows that the structurally optimized, nearly tetrahedral geometry at the missing H site does not change

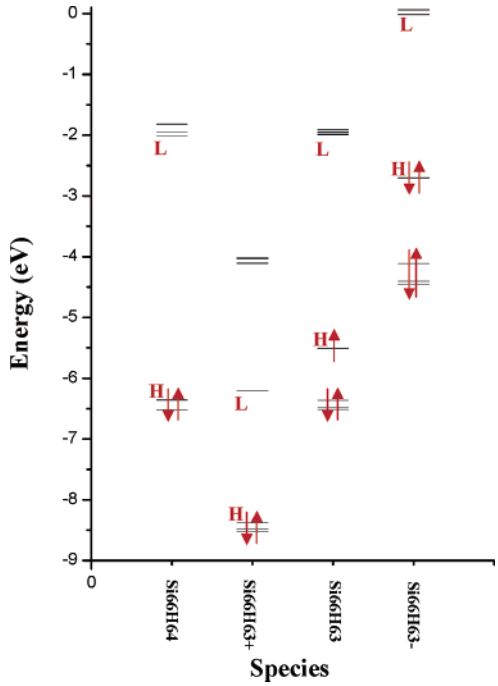


***Figure 7.*** Energetics of frontier orbitals of charged $Si_{66}H_{63}$.

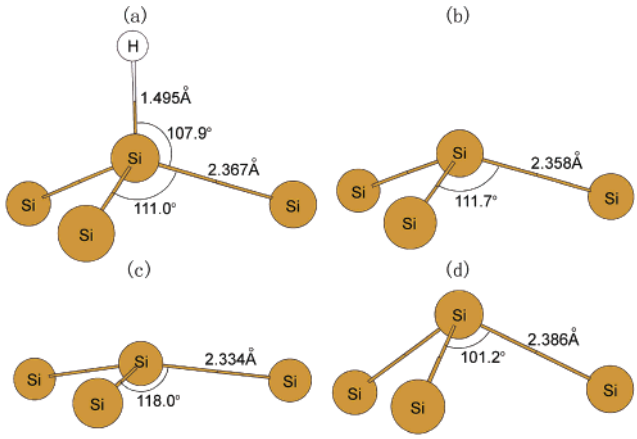


***Figure 8.*** Local structures of parent nanocrystal $Si_{66}H_{64}$ and charged $Si_{66}H_{63}$ radicals. (a) $Si_{66}H_{64}$, (b) $Si_{66}H_{63}$ neutral radical, (c) $Si_{66}H_{63}^{+}$ radical cation, (d) $Si_{66}H_{63}^{-}$ radical anion.

significantly when H is removed. However, if the lone pair electron is removed in the cation, the Si−Si bonds strengthen and shorten, moving toward a planar configuration of 120 degree Si−Si bond angles. In the anion, the bonds weaken and lengthen, with the angle moving toward a pyramidal 90° angle. These changes create substantial reorganization energies of 0.5 eV for the radical ionization potential and electron affinity, as shown in Table 3. This is in contrast to the cation and anion of the parent nanocrystal, which show small reorganization energies for electron transfer into delocalized HOMO and LUMO states.

As we have seen, the radical nanocrystal can be observed by its ESR signal. Optical spectroscopy in principle is a more sensitive detection method. The static DFT calculated optical transitions (Supporting Information) show that radical $Si_{66}H_{63}$ should have strongly allowed absorption transitions, involving the surface state, at around 1.0 and 3.5 eV. These transitions are at much lower energy than those of the parent nanocrystal. This calculation indicates that the 0.9-eV emission seen at low

(48) Meyer, B. K.; Hofmann, D. M.; Stadler, W.; Petrovakoch, V.; Koch, F.; Omling, P.; Emanuelsson, P. *Appl. Phys. Lett.* **1993**, *63*, 2120.
(49) Fujii, M.; Mimura, A.; Hayashi, S.; Yamamoto, K.; Urakawa, C.; Ohta, H. *J. Appl. Phys.* **2000**, *87*, 1855.

***Table 3.*** Properties of Structurally Optimized Doped $Si_{66}$ Nanocrystals As Described in the Text[a]

| species | $Si_{66}H_{64}$ | $Si_{66}H_{63}$ | $Si_{65}$(coreAl)$H_{64}$ | $Si_{65}$(coreP)$H_{64}$ | $Si_{65}H_{63}$(Psurf) | $Si_{65}H_{64}$(Psurf) | $Si_{65}$(coreP)$H_{63}$ |
|---|---|---|---|---|---|---|---|
| symmetry of optimized species | Td | C3v | Cs | C3v | C3v | C3v | C3v |
| HOMO | −6.36 | −5.51 | −6.08 | −3.46 | −5.97 | −3.21 | −4.72 |
| symmetry of HOMO | T2 | A1 | App | A1 | A1 | A1 | A1 |
| LUMO | −2.02 | −1.99 | −1.99 | −2.08 | −2.04 | −2.03 | −2.69 |
| symmetry of LUMO | A1 | E | Ap | E | A1 | A1 | A1 |
| LUMO−HOMO gap | 4.34 | 3.51 | 4.09 | 1.37 | 3.94 | 1.18 | 2.03 |
| adiabatic ionization energy $\mathbf{I_a}$ | 7.07 | 5.65 | 6.43 | 4.02 | 6.51 | 3.79 | 4.97 |
| vertical ionization energy $\mathbf{I_v}$ | 7.15 | 6.16 | 6.78 | 4.22 | 6.80 | 4.02 | 5.50 |
| hole reorganization energy $\lambda_\mathbf{h}$ | 0.08 | 0.51 | 0.35 | 0.20 | 0.30 | 0.24 | 0.53 |
| adiabatic electron affinity $\mathbf{A_a}$ | 1.34 | 3.09 | 4.39 | 2.00 | 1.32 | 1.87 | 2.14 |
| vertical electron affinity $\mathbf{A_v}$ | 1.25 | 2.59 | 4.10 | 1.80 | 1.26 | 1.49 | 2.02 |
| electron reorganization energy $\lambda_\mathbf{e}$ | 0.08 | 0.50 | 0.28 | 0.20 | 0.06 | 0.37 | 0.12 |
| Fermi energy | −4.20 | −4.37 | −5.44 | −3.01 | −4.03 | −2.76 | −3.76 |
| absolute hardness | 5.90 | 3.58 | 2.67 | 2.42 | 5.54 | 2.53 | 3.48 |
| dipole moment (Debye) | 0.00 | 0.12 | 1.41 | 0.82 | 0.41 | 1.11 | 9.62 |

[a] All energies are in eV. All species were optimized at the 6-31G* level, with final energies calculated at the 6-31G* level, too.

temperature[49] is a luminescence involving a surface electron recombining with a hole in the delocalized parent HOMO.

The radical nanocrysal has an adiabatic electron affinity of 3.09 eV, significantly more than the 1.34 eV value of parent $Si_{66}H_{64}$. It acts as a deep electron trap, and might pick up a mobile electron in an electronic material. The resulting radical anion nanocrystal would show no ESR signal, and have a strong low-lying allowed optical absorption at about 2.7 eV. The radical nanocrystal also has a lower adiabatic ionization energy than the parent nanocrystal (5.65 eV vs 7.07 eV), and thus would be a deep trap for mobile holes. The radical cation nanocrystal would have a very strong transition near 2.3 eV, and also would have no ESR signal. We suggest that significant numbers of radical cation and anion nanocrystals exist in nanocrystal materials such as porous Si, in addition to the neutral radical nanocrystals seen by ESR.

**B. Electrical Doping.** The column III and V elements Al and P contain one less or more valence electron than column IV Si, and are used to electrically dope Si with holes or electrons in Si devices. In the bulk crystal they replace Si in the lattice and show $sp^3$ hybridization, with the extra carrier weakly bound to the impurity atom in a large 3-nm radius hydrogenic orbital. At 23 °C, the extra hole or electron is thermally ionized, and carries current under an applied electric field. In nanocrystals the dopant atom could be either inside, or on the surface with possibly a different hybridization. The extra carrier's wave function and binding energy will be strongly modified by finite nanocrystal size. In larger nanocrystals, quantum confinement changes the ESR hyperfine spectrum on a dopant P atom.[50] This change has been modeled using quantum size and continuum electrostatic approaches. Nanocrystals with one dopant atom have an odd number of electrons, and may resemble radical nanocrystals in some respects.

There is an interesting experimental connection between luminescence, dangling bonds, and doping.[51−54] The effect of P doping has been studied in oxide films containing oxide passivated Si (also SiGe alloy) nanocrystals emitting near 1.4 eV on their band gap transitions. Luminescence increases, and the ESR dangling bond signal decreases, as P content initially increases. Although the structural location of P is not known, a possible mechanism is electron transfer from a P atom dopant to the surface dangling bond, creating a lone pair which does not show an ESR signal or trap the optically excited electron.

In view of these results, we study doped nanocrystals, with and without a surface dangling bond. In odd electron, hole doped $Si_{65}$(core Al)$H_{64}$, we replace one internal Si with Al (Table 3 and Figure 6e); the structure converges with substitutional Al on the Si lattice site. In the parent nanocrystal $Si_{66}H_{64}$ this specific Si atom is closer to one surface than the others as shown in Figure 9b, and has a slightly shorter (0.015 Å) bond length in the direction toward this surface. In Figure 9a, the structurally optimized substitutional Al has two short and two long bonds to neighboring Si, with a further slight asymmetric caused by the nearly surface. Figure 6e shows the resulting hole is closely localized on two longer Si−Al bonds. This empty level lies not in the band gap, but essentially degenerate with the highest occupied delocalized nanocrystal level as shown in Figure 10. As expected the Fermi level moves down, to −5.44 eV, and the adiabatic electron affinity increases to 4.39 eV. For spectroscopic identification purposes, this species would have an ESR signal but no allowed optical transitions below 4.0 eV.

In the corresponding electron doped $Si_{65}$(core P)$H_{64}$, the extra electron lies in the gap 1.42-eV below the LUMO of the parent nanocrystal in Figure 10. The substitutional P atom has one short Si−P atom in the direction of the surface, and three longer Si−P bonds in the perpendicular plane in the Figure 9c. The spatial distribution of the extra electron around P is along three longer Si−P bonds in Figure 6d. The Fermi energy increases to −3.01 eV, and the ionization potential is only 4.02 eV. As the electron affinity of the Al doped nanocrystal is higher than the ionization potential of the P doped nanocrystal (see Table 3), the calculation indicates that there would be spontaneous electron transfer from P to Al, regardless of whether they were in the same or different nanocrystals. In these doped species, the cation and anion reorganization energies are midway between those of the localized radical nanocrystal, and the parent $Si_{66}H_{64}$ nanocrystal.

In the even electron nanocrystal $Si_{65}H_{63}$(Psurf), a surface Si−H group is replaced with P. Intuitively, the P atom here

(50) Fujii, M.; Mimura, A.; Hayashi, S.; Yamamoto, Y.; Murakami, K. *Phys. Rev. Lett.* **2002**, *89*, 206805.
(51) Mimura, A.; Fujii, M.; Hayashi, S.; Kovalev, D.; Koch, F. *Phys. Rev. B* **2000**, *62*, 12 625.
(52) Toshikiyo, K.; Tokunaga, M.; Takeoka, S.; Fujii, M.; Hayashi, S.; Moriwaki, K. *J. Appl. Phys.* **2001**, *90*, 5147.
(53) Toshikiyo, K.; Tokunaga, M.; Takeoka, S.; Fujii, M.; Hayashi, S. *Physica B* **2001**, *308*, 1100.
(54) Makimura, T.; Yamamoto, Y.; Mitani, S.; Mizuta, T.; Li, C. Q.; Takeuchi, D.; Murakami, K. *Appl. Surf. Sci.* **2002**, *197*, 670.

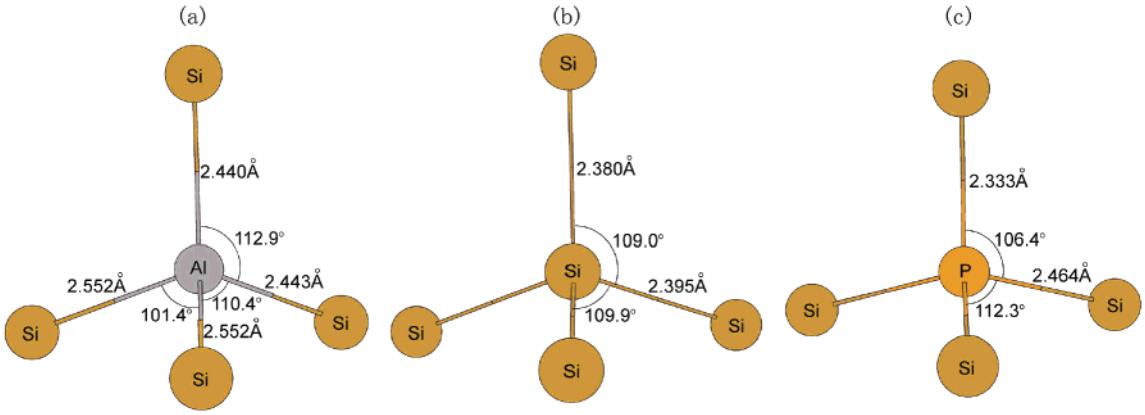


***Figure 9.*** Local structures of parent nanocrystal $Si_{66}H_{64}$ and interior doped $Si_{66}$ nanocrystals. (a) $Si_{65}$(core Al)$H_{64}$, (b) $Si_{66}H_{64}$, (c) $Si_{65}$(core P)$H_{64}$.

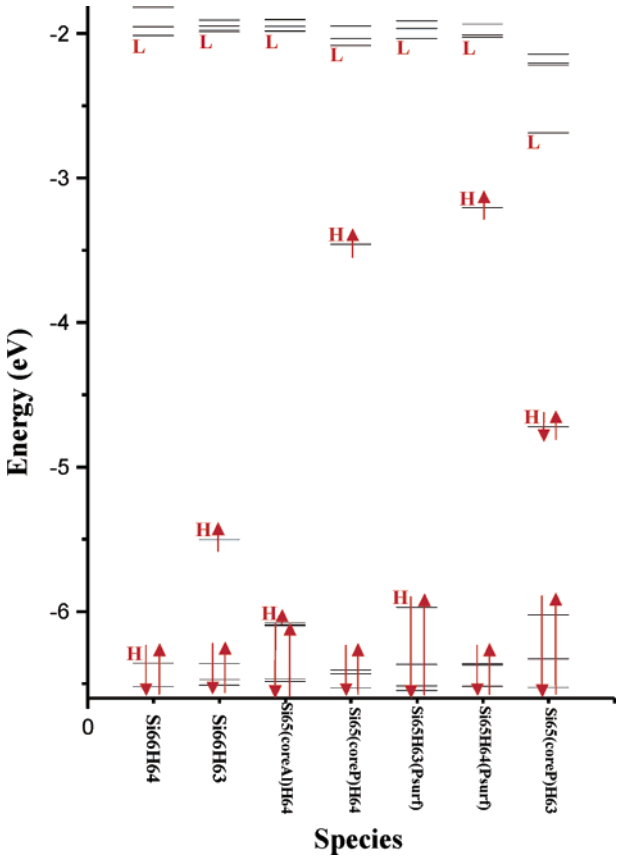


***Figure 10.*** Energetics of frontier orbitals of doped $Si_{66}$ nanocrystals.

should show three covalent bonds to neighboring Si atoms, and a singlet lone pair pointing outward. The calculation converges to this result, with the doubly occupied lone pair lying deep in the gap 0.4 eV above the HOMO of the parent nanocrystal in Figure 10. This nanocrystal has electrical properties similar to its parent, and is not doped. A strongly allowed transition lies at about 3.9 eV. The Si−P bond lengths are 2.312 Å. In the odd electron species $Si_{65}H_{64}$(Psurf), the surface P shows $sp^3$ hybridization when bonded to an extra H atom in Figure 11b. This structure is stable against PH bond dissociation. This nanocrystal is effectively doped with electronic properties similar to the previously discussed $Si_{65}$(core P)$H_{64}$. The extra electron lies 1.19 eV below the LUMO of the parent nanocrystal, and spatially resides on the Si−P bonds in Figure 6f. There is a very strong optical transition at 1.2 eV. This calculation shows that surface P can act as a dopant if it is capped with H.

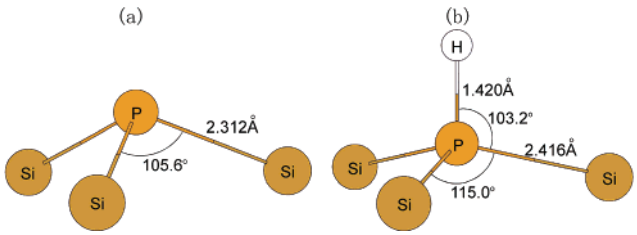


***Figure 11.*** Local structures of (a) $Si_{65}H_{63}$(Psurf) and (b) $Si_{65}H_{64}$(Psurf).

The even electron $Si_{65}$(core P)$H_{63}$ nanocrystal is core P doped near one surface, and has a missing H radical site on the opposite surface across the nanocrystal. The calculation converges to a ground state with an electron lone pair at the missing H atom in Figure 6a, similar to the radical anion nanocrystal. An electron has transferred from the P localized orbital to the radical localized orbital. The HOMO−LUMO gap, corresponding in this case to electron promotion across the nanocrystal to the empty P localized orbital, is 2.03 eV. This species would have no ESR spectrum, and a series of weakly allowed transitions in the 2.0−3.5 eV range. The intensity of these transitions should decrease with increasing distance between donor and acceptor. This result is generally consistent with the prior proposal in luminescence studies that the P electron will transfer to, and pair with, the radical extra electron.[49−54]

The ionization potential of the PH donor nanocrystal $Si_{65}H_{64}$-(Psurf) is 3.79 eV—quite low—but still higher than the electron affinity of the radical nanocrystal 3.09 eV. In a vacuum when the nanocrystals are at infinite separation, transfer is endothermic. If there were no charging energies for the nanocrystals after transfer, then transfer would be exothermic, because the PH donor level lies 2.3 eV above the radical level when both are referenced to vacuum in Figure 10. If the nanocrystals were embedded in a medium of modest dielectric constant, charging energies would decrease and transfer is likely to be exothermic. Even in a vacuum, if the radical and PH groups on separate nanocrystals are very close in space, facing each other, then the resulting Coulomb attract may make the electron-transfer exothermic.

## Discussion and Conclusion

Our calculations on different types of $sp^3$ chemical passivation schemes show that H termination creates both the highest HOMO−LUMO gap and the largest electron transfer hardness (i.e., quasiparticle band gap). H passivated nanocrystals also most closely follow the simple quantum size effect model in

the spatial distribution of the HOMO and LUMO, as well as in the size dependence of the band gap and the ionization potentials. The H atom electronegativity is close to that of Si (2.1 vs 1.8); matching of electronegativity creates the physical situation for this model to be valid. By contrast, alkane passivation increases the nanocrystal Fermi energy, while F atom passivation lowers the Fermi energy, as might be expected from simple electronegativity considerations. In thin $SiO_2$ shell passivation, we find that simple OH termination is a useful approximation for thicker oxide surface layers. For the $Si_{35}$ nanocrystal, the oxide passivation band gap is a factor of 2 lower than the H passivation band gap: this difference is not sensitive to the exact bonding, thickness, or strain in the oxide. Oxide passivation creates a specific chemical shift with respect to H passivation: the HOMO moves up and the LUMO moves down. This result explains the experimental observation that small Si nanocrystals emit in the red when oxide passivated, and in the blue when H passivated. In all of the nanocrystals where there is a strong electronegativity difference between Si and the passivating atoms, the HOMO tends to concentrate (while remaining delocalized) on the weakened interfacial Si−Si "backbonds".

Electron-transfer reorganization energies are on the order of 0.1 eV for these nanocrystals, as might be expected from the weak nature of electron-vibrational coupling in crystalline Si. The HOMO and LUMO are delocalized, and the LUMO of the neutral is very similar to the HOMO of the anion. However, in nanocrystals with a dangling bond surface state, there is a 0.5 eV reorganization energy and significant localized bonding change upon nanocrystal charging.

P and Al atoms directly substituted onto Si lattice sites create stable nanocrystal species that have Fermi level shifts as expected from bulk crystalline doping electronegativity considerations. However, the extra hole or electron is not delocalized as in the bulk dopant Wannier wave function, but instead concentrates on bonds directly involving the impurity P or Al atom. In a nanocrystal with both a P dopant atom and a dangling bond, the P extra electron transfers to the dangling bond in the ground electronic state. This result is consistent with experimental observations that P doping increases nanocrystal luminescence in ensemble samples where some nanocrystals have surface dangling bonds.

**Acknowledgment.** We thank M. Hybertsen and M. Steigerwald for extensive discussion and useful suggestions. L.B. also thanks M. Head-Gordon, G. Galli, A. Williamson, and J. Grossman for stimulating discussions of DFT and TDDFT methods. This work has been supported by the Department of Energy, Basic Energy Sciences, under DEFG0298ER14861 and DEFG0290ER14162. This work was supported in part by the Columbia MRSEC Program of the National Science Foundation under Award No. DMR-0213574 and National Computational Science Alliance under Grant No. MCA95C007N and utilized the IBM P690. A portion of the research described in this paper was performed in the Environmental Molecular Sciences Laboratory, a national scientific user facility sponsored by the Department of Energy's Office of Biological and Environmental Research and located at Pacific Northwest National Laboratory.

**Supporting Information Available:** Calculated static optical transitions for species as described in the text. This material is available free of charge via the Internet at http://pubs.acs.org.

JA036443V